

Letter of Intent

Neutrino Oscillation Experiment at JHF

Summary

The next generation long baseline neutrino experiment from JHF to Super Kamiokande with a baseline length of 295 km is proposed to explore the physics beyond the Standard Model.

The beam power of JHF PS is capable of delivering 3.3×10^{14} 50 GeV protons every 3.5 seconds (0.75 MW). The experiment assume 130 days of operation at full intensity for five years. The high intensity neutrino beam is produced by off-axis configuration. The peak neutrino energy is tuned to the oscillation maximum of ~ 0.8 GeV to maximize the sensitivity on the neutrino oscillation.

The merits of this experiment can be summarized as follows.

- The off-axis beam can produce the highest possible intensity with narrow energy spread. The oscillation maximum will be ~ 0.8 GeV for the distance (290 km) and $\Delta m^2 \sim 3 \times 10^{-3} \text{eV}^2$. The corresponding angle of the beam line axis relative to the direction of far detector is about 2 degree.
- The far detector already exist. SK has excellent performance to detect low energy neutrinos.
- The neutrino events at sub-GeV are dominated by the charged current quasi-elastic interaction, where the neutrino energy E_ν can be reconstructed by two body kinematics.
- The experience in SK operation and analysis tool already exist.

The expected sensitivities, assuming 0.75 MW 130 days operation for five years are:

- Discovery of $\nu_\mu \rightarrow \nu_e$ at $\Delta m^2 \sim 3 \times 10^{-3} \text{eV}^2$ down to $\sin^2 2\theta_{13} \sim 0.006$. This is a factor of twenty improvement of the sensitivity.
- The precision measurements of oscillation parameters in ν_μ disappearance down to $\delta(\Delta m_{23}^2) = 10^{-4} \text{eV}^2$ and $\delta(\sin^2 2\theta_{23}) = 0.01$
- Search for sterile components in ν_μ disappearance by detecting the neutral current events

With a successful completion of the first stage, the second stage of the experiment will be envisaged. In the second stage with 1 Mt Hyper-Kamiokande and upgraded 4 MW PS, ν_e CP Violation in lepton sector can be searched, if $\sin^2 2\theta_{13}$ is in the discovery range of the first stage of the experiment. Sensitivity in the proton decay search is significantly improved upto 10^{35} (3×10^{34}) years in life time for the $p \rightarrow e^+ \pi^0$ ($p \rightarrow \bar{\nu} K^+$) mode.

1 Participating Institutes and participants and Possible contributions

Contents

| | | |
|----------|--|-----------|
| 1 | Participating Institutes and participants and Possible contributions | 2 |
| 2 | Physics goal of the JHF neutrino project | 4 |
| 2.1 | History | 4 |
| 2.2 | Merits of the JHF physics program | 4 |
| 2.3 | The present understanding of neutrino mass and mixing | 5 |
| 2.4 | The goal of first stage of the neutrino experiment at JHF | 6 |
| 3 | Neutrino beam at JHF | 7 |
| 4 | Near detectors | 10 |
| 4.1 | Muon monitor | 10 |
| 4.2 | Near detector at 280m from the target | 10 |
| 5 | Intermediate detector | 11 |
| 6 | Far detector: Super-Kamiokande | 13 |
| 7 | Physics in the first stage of the project | 14 |
| 7.1 | High precision measurement of Δm_{23}^2 and θ_{23} with ν_μ disappearance | 14 |
| 7.2 | ν_e appearance search | 15 |
| 7.3 | Search for sterile neutrinos (ν_s) in ν_μ disappearance | 17 |
| A | Neutrino oscillation | 19 |
| B | Physics in the future extension with Hyper-Kamiokande | 21 |
| B.1 | Discovery potential of CP violation in the lepton sector | 22 |
| B.2 | Sensitivity of proton decay | 24 |

2 Physics goal of the JHF neutrino project

The main physics motivation of the JHF neutrino project is to explore physics at much higher energy scale than that can be done by collider experiments in near future. The studies of the atmospheric and solar neutrinos have shown that neutrinos have masses and have large mixings. The confirmation of the existence of neutrino oscillations by the first generation experiments must be followed by the precision measurements of the neutrino oscillation parameters. The neutrino mass and mixing can be one of a few possible windows of physics at near Grand Unification energy scale. A massive detector, which is essential to have enough statistics for neutrino physics, is also important for the search and studies of the proton decay. The proton decay is a direct evidence of unification of quark and lepton. In addition, the comparison of the neutrino and anti-neutrino oscillations are the only possible way to search for the leptonic CP violation with presently available technologies. The proton instability and CP violation may lead us to the understanding of the baryon anti-baryon asymmetry in the universe [1].

2.1 History

The neutrino program has been one of the main motivations of building high intensity proton synchrotron since the JHF project was first discussed in 1995. The possible neutrino experiment was first discussed in 1996 at INS symposium, and at JAERI in 1997 at JAERI workshop. Due to the rapid progress of neutrino physics in the world, it became necessary to re-evaluate the physics goals for the next generation neutrino oscillation experiment. The JHF neutrino experiment working group was formed in 1999 to formulate our strategy. The results of the studies was reported at a workshop of Japanese high-energy physics community and the Expression of Interest was submitted to the JHF project team in January 2000. The LOI was published in 2001 [2].

In 2002, two international workshop was held. The attendants include physicists from Canada, France, Italy, Korea, Russia, Spain and US and an international working group has been formed. This LOI is the summary of old LOI with updates for recent new developments.

2.2 Merits of the JHF physics program

The physics program consists of two stages of the experiments. This LOI is for the first stage of the program. The feasibility of the entire physics program depends on the results of first stage. The JHF neutrino experiment (JHFnu) has the following merits.

- The far detector

JHFnu will use the world largest water Čerenkov detector, Super-Kamiokande (SK) as the far detector in the initial stage. Super-Kamiokande has excellent energy resolution and e/μ identification capability in low energy neutrino reactions, where the multiplicity of the final state particles is small.

- The neutrino beam energy

The maximum sensitivity of the oscillation parameters can be achieved by tuning the neutrino beam energy to the oscillation maximum. The oscillation maximum will occur at the neutrino energy E_ν less than 1 GeV for the 295 km baseline with $\Delta m^2 \sim 3 \times 10^{-3} eV^2$. This neutrino energy is well mated to the detector capability.

- E_ν reconstruction

The charged current interaction is dominated by the quasi-elastic interaction (CCQE) below 1 GeV. This enables us a precision determination of the neutrino energy of both ν_μ and ν_e . The energy can be calculated by a formula:

$$E_\nu = \frac{m_N E_l - m_l^2/2}{m_N - E_l + p_l \cos \theta_l}, \quad (1)$$

where m_N and m_l is the mass of the neutron and the lepton (=e or μ), and E_l , p_l and θ_l are the energy, momentum, and angle of the lepton relative to the neutrino beam, respectively.

- Backgrounds

The precision of the oscillation parameters is limited mainly due to high-energy components. The inelastic reactions of high-energy neutrinos constitute the backgrounds to the CCQE, which is used to measure neutrino energy. In addition, the inelastic reactions produce π^0 that is the main backgrounds for electron appearance search. The sub-GeV neutrino beam with small high-energy tail is required from the backgrounds consideration.

- Off-axis beam

The experiment will use off-axis beam to accomplish the highest possible intensity of low energy and small high-energy tail in the spectrum.

- Start up of the experiment

SK has been in operation for many years and the relevant software already exists. The intensity of the low energy neutrino beam is proportional to the proton beam power and does not require specific proton energy in the initial operation of the accelerator. The experiment will be accommodating reasonable start up scenario of accelerator and can produce physics results in a short time after initial operation.

2.3 The present understanding of neutrino mass and mixing

The recent progress of neutrino physics can be summarized as follow. In the three neutrino scheme, the neutrino oscillation can be described by five parameters: three mixing angles $\theta_{12}, \theta_{23}, \theta_{13}$ between weak eigen-state and mass eigen-states, one CP phase δ , and two independent mass squared differences, $\Delta m_{21}^2 (= m_2^2 - m_1^2)$ and $\Delta m_{32}^2 (= m_3^2 - m_2^2 \sim \Delta m_{31}^2)$ [3] [4]. There are two strong evidences of neutrino oscillation and one result remains to be examined.

1. Oscillation of $\nu_\mu \rightarrow \nu_\tau$ with $\Delta m^2 \sim 3 \times 10^{-3} eV^2$ (Δm_{23}^2)

- Super-Kamiokande collaboration [5] showed that the rate of upward-going ν_μ is about one-half of the expected. The corresponding oscillation parameters are $1.6 \times 10^{-3} eV^2 < \Delta m^2 < 3.9 \times 10^{-3} eV^2$, $\sin^2 2\theta > 0.92$ at 90% CL.
- The K2K collaboration [6] showed that the reduction of ν_μ flux with more than 99% confidence level. The results also show the indication of the energy spectrum distortion during the 250 km flight path from KEK and Kamioka. The resultant oscillation parameters are consistent with atmospheric neutrino observation. If confirmed with more statistics, this is the direct evidence of neutrino oscillation in ν_μ disappearance at $\Delta m^2 \sim a few \times 10^{-3} eV^2$.

- The most likely source of the ν_μ rate reduction is due to $\nu_\mu \rightarrow \nu_\tau$ oscillation, based on the atmospheric neutrino observations in Super-Kamiokande [7]. The confirmation can be expected by CERN-Gran-Sasso project by identifying the production of tau lepton. The experiment is scheduled to start in 2006.
2. Oscillation $\nu_e \rightarrow \nu_\tau$ and $\rightarrow \nu_\mu$ with $\Delta m^2 \sim 10^{-4} eV^2$ mass region (Δm_{12}^2)
 - The SNO [8] collaboration announced their results on solar neutrino (ν_e) observation. The results show ν_μ and ν_τ components exist in solar neutrinos. This is the direct evidence of neutrino oscillation in solar neutrinos.
 - Combining all the solar neutrino experiments, the Large Mixing Angle (LMA) solution is preferred [9]. The oscillation parameters are $2.5 \times 10^{-5} eV^2 < \Delta m^2 < 3.3 \times 10^{-4} eV^2$, $0.25 < \tan^2 \theta < 0.9$ at 3σ bounds.
 - The Kamland [10] observed the rate reduction of reactor neutrinos ($\bar{\nu}_e$) in the flight path of about 200 km with 4.6σ , thus confirm the solar neutrino results of LMA solution.
 3. In the above oscillations, there is no indication of the existence of sterile neutrinos at the level of 20% to 30%.
 4. $\Delta m^2 \sim 10^{-1} eV^2$ region
 - LSND collaboration reported an evidence of neutrino oscillation in $\bar{\nu}_\mu \rightarrow \bar{\nu}_e$ in $\Delta m^2 \sim 10^{-1} eV^2$ region. But similar experiment, KARMEN collaboration did not see the effect with slightly less sensitivity. If confirmed, LSND effect requires fourth kind of neutrino, which does not interact with Z-boson to be consistent with LEP experiments.
 - Mini-BooNE experiment has started at Fermilab either to confirm or to refute the LSND effect. The results will be available in a few years.

The next generation experiment should have a high sensitivity/precision to study physics in lepton sector with much more powerful and well controlled neutrino beam and should proceed beyond 'confirmations' of neutrino oscillation.

2.4 The goal of first stage of the neutrino experiment at JHF

The first stage of the experiment has three main goals:

1. The discovery of $\nu_\mu \rightarrow \nu_e$ at $\Delta m_{13}^2 (\sim \Delta m_{23}^2)$

A factor of 20 more improvement of sensitivity over the present upper limit is possible in five years operation with full operation of JHF accelerator. The goal is to extend the search down to $\sin^2 2\theta_{13} \simeq 2 \sin^2 2\theta_{\mu e} > 0.006$. This measurement is important for two reasons.

 - The mixing angle θ_{13} is the last of the mixing angles in three neutrinos scheme.
 - This is an appearance channel and a sub-leading oscillation of ν_μ with Δm_{13}^2 .
The new developments in solar and reactor neutrino experiments indicate that ν_μ will oscillate to ν_e with a rather large mixing angle with Δm_{12}^2 . This oscillation can compete with the one with a mass squared difference of Δm_{13}^2 . The former oscillation will be suppressed by small Δm^2 and the latter is suppressed by small mixing angle θ_{13} . Two

processes can be comparable in strength. This is the necessary condition for CP violation effect to be observable.

2. The precision measurements of oscillation parameters in ν_μ disappearance

The observation of oscillation minimum and 1% measurement (about the same precision as Cabbibo angle in quark sector) of the mixing angle and 10% measurement of Δm^2 ($\delta(\Delta m_{23}^2) = 10^{-4} \text{ eV}^2$ and $\delta(\sin^2 2\theta_{23}) = 0.01$) may show the mixing of second and third generation of neutrinos to be maximal to 99% level. This may impose a constraint on the quark-lepton unification in the future.

3. Search for sterile components in ν_μ disappearance by detecting the neutral current events

If a non-zero sterile component is found, the physics of Fermions need modification to accommodate extra member(s) of lepton.

With the successful achievements of the first stage measurements, the construction of 1 Mt Hyper-Kamiokande detector at Kamioka, and a possible upgrade of the accelerator from 0.75 MW to 4 MW in beam power, further experiments can be envisaged. That include another order of magnitude improvement in the $\nu_\mu \rightarrow \nu_e$ oscillation sensitivity, a sensitive search of the CP violation in the lepton sector (CP phase δ down to $10^\circ - 20^\circ$), and an order of magnitude improvement in the proton decay sensitivity.

3 Neutrino beam at JHF

The proton beam is fast-extracted from the 50 GeV PS in a single turn and transported to the production target. The design intensity of the PS is 3.3×10^{14} protons/pulse (ppp) at a repetition rate of 0.285 Hz (3.5 second period), resulting in a beam power of 0.75 MW (2.64 MJ/pulse). The spill width is $\sim 5.2 \mu\text{sec}$. We define a typical one year operation as 10^{21} protons on target (POT), which corresponds to about 130 days of operation. The intensity of the low energy neutrino is almost proportional to the proton beam power (proton energy \times total number of protons per sec.). For the start up period of the accelerator, where the flux may be expected low, the performance of the experiment should be down graded by the available beam power but can produce physics results accordingly.

The distance is 295 km between JHF at Tokai and Super-Kamiokande at Kamioka. With 295 km baseline, the neutrino energy will be tuned to between 0.4 and 1.0 GeV, which corresponds to Δm^2 between 1.6×10^{-3} and $4 \times 10^{-3} \text{ eV}^2$ suggested by the recent Super-Kamiokande result and K2K [?] [6].

The layout of JHF facility is drawn in Figure 1. The protons are extracted toward inside of the PS ring, and are bent by 90° to SK direction by the transport line with a radius of curvature of 110 m. We will adopt superconducting magnets for the transport line. The secondary pions (and kaons) from the target are focused by horns magnet [11], and decay in the decay pipe. The length of the decay pipe from the target position is 130 m. The first front detector is located at 280 m from the target.

We adopt the off axis beam (OAB) configuration. The OAB is the method to produce a narrow neutrino energy spectrum [12]. The axis of the beam optics is displaced by a few degree from the far detector direction (off-axis). With a finite decay angle, the neutrino energy becomes almost independent of parent pion momentum due to a characteristics of the Lorenz boost, thus provides

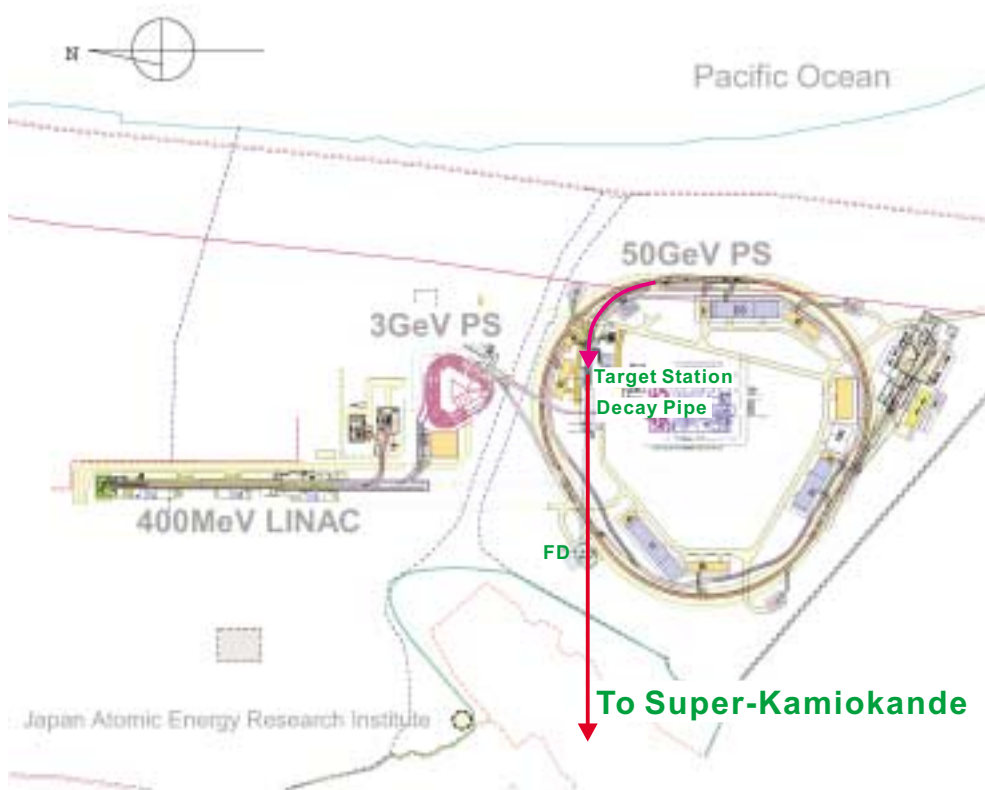


Figure 1: Layout of JHF.

Table 1: Summary of ν_μ beam simulation. The peak energy E_{peak} is in GeV. The flux is given in $10^6/\text{cm}^2/\text{yr}$, and the ν_e/ν_μ flux ratio is in %. The ratio in the “total” column is the one integrated over neutrino energy and the column “ E_{peak} ” is the ratio at the peak energy of ν_μ spectrum. The normalization for the number of interactions are /22.5kt/yr. The numbers outside (inside) the bracket are number of total (CC) interactions.

| Beam | E_{peak} | Flux | | $\nu_e/\nu_\mu(\%)$ | | # of interactions | |
|------|------------|-----------|---------|---------------------|------------|-------------------|---------|
| | | ν_μ | ν_e | total | E_{peak} | ν_μ | ν_e |
| OA2° | 0.7 | 19.2 | 0.19 | 1.00 | 0.21 | 3100(2200) | 60(45) |
| OA3° | 0.55 | 10.6 | 0.13 | 1.21 | 0.20 | 1100(800) | 29(22) |

the narrow spectrum. The peak neutrino energy can be adjusted by choosing the off-axis angle. ν_μ and $\bar{\nu}_\mu$ can be switched by flipping the polarity of the horn magnets.

Monte-Carlo (MC) simulations using GEANT [13] have been used to estimate expected neutrino spectra and number of events. The target is assumed to be simple Carbon rod of 1-cm diameter and 1-m long. The Calor-Fluka model [14], which is known to work better at higher energies, is used in the present simulation. From the observed of neutrino events rate at near detector of K2K, the beam MC is known to provide absolute neutrino flux with an error less than 20%.

Fig. 2(left) shows expected neutrino energy spectrum of charged current interactions at Super-Kamiokande. Fluxes and numbers of interactions are summarized in Table 1. The OAB is roughly a factor of three more intense than possible momentum selected beam. The ν_e contamination in the beam are expected to be 1% at the off-axis angle of 2° (OA2°). The sources of ν_e are $\pi \rightarrow \mu \rightarrow e$ decay chain and K decay (K_{e3}). Their fractions are μ -decay: 37%, K-decay: 63% for OA2°. The energy spectra of the ν_e contamination are plotted in Fig. 2(right). At the peak energy of ν_μ spectrum, the

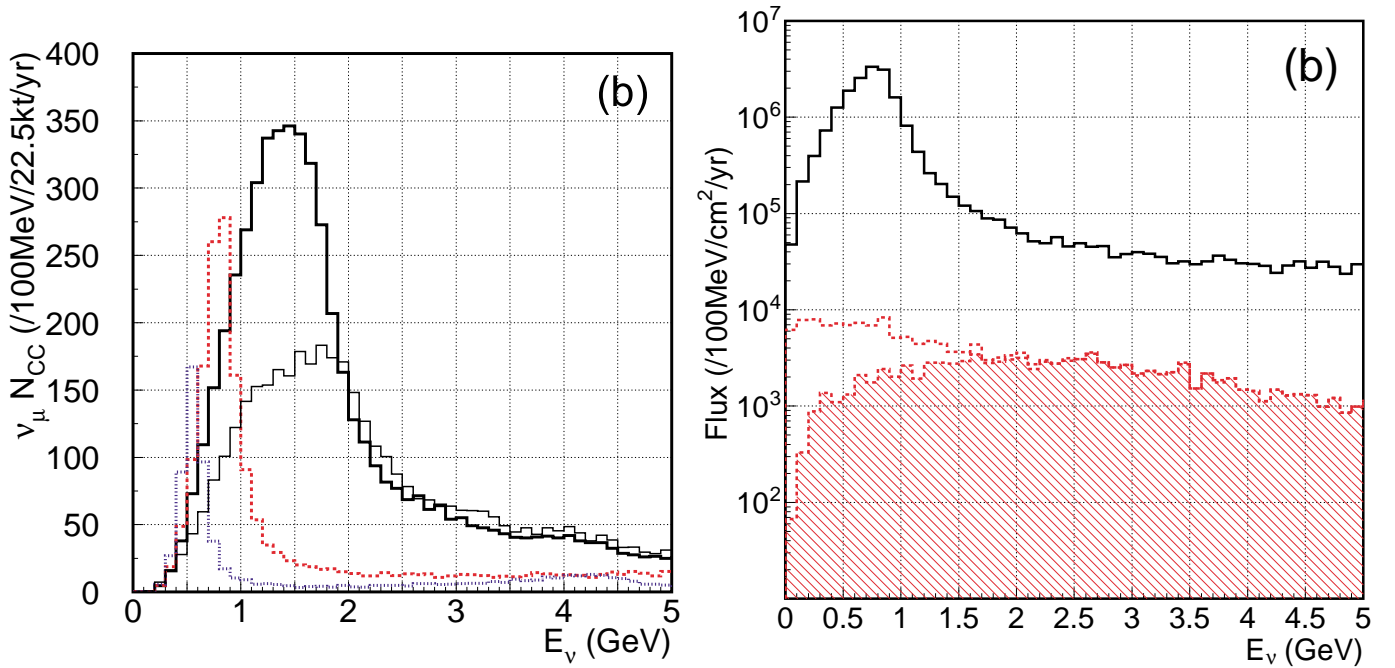


Figure 2: Left: Neutrino energy spectra of charged current interactions. Thick solid, dashed and dotted histograms are OA1°, OA2° and OA3°, respectively. Right: Comparison of ν_e and ν_μ spectra OA2°. Solid (black) histogram is ν_μ and dashed (red) one is ν_e . Hatched area is contribution from K decay.

ν_μ/ν_e ratio is as small as 0.2% in OAB. This indicates that beam ν_e background is greatly suppressed (factor ~ 4) by applying energy cut on the reconstructed neutrino energy.

Finally, we mention an option of the off-axis beam. One disadvantage of the off-axis beam is a relative difficulty in changing the neutrino beam energy after constructing the beam line. The beam line must be re-aligned, if one wants to change the beam energy. A relatively easy method to change the neutrino beam energy after finishing the beam line construction is to install a bending magnet after the horns. Detailed Monte Carlo studies have been carried out to study the effect of the bending magnet on the neutrino flux. In the present study, the primary beam line was aligned 2.6 degree off-axis, and the secondary beam was bent toward or against the far detector. The Monte Carlo results show that the neutrino flux by this scheme and the conventional off-axis scheme is almost identical for off-axis angles between 2 and 3 degrees. Therefore, we are seriously considering this scheme as a possible beam line option, and various engineering studies are in progress.

One of the sources of systematic uncertainties is the near to far extrapolation of neutrino spectrum. In Figure 3, spectra at far and near sites are compared. The peak position is shifted to higher energy at the far site than at the near site. The far/near spectrum ratio is also plotted in the figure. The difference is as large as 40~50%. The sources of this far/near difference are the difference in the solid angle between far and near detectors and the finite length of decay pipe; the neutrino source is point like for the far detector, but the length of the decay pipe is not negligible for the near detector. At the distance longer than one km from the target, both of the above two effects become negligible and the far/near ratio becomes flat.

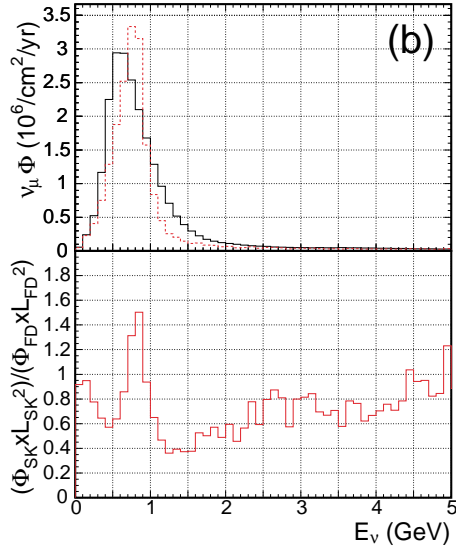


Figure 3: Comparison of spectra at far and near site for OA2°. Upper figure is ν_μ spectra at 280 m (solid black histogram) and 295 km (dashed red histogram). The flux for the near site is multiplied by $(295/0.28)^2$ to directly compare the spectra. The front detector size is assumed to be ± 5 m in horizontal and vertical directions. The lower plots are far/near ratio of fluxes.

4 Near detectors

4.1 Muon monitor

The direction of the proton beam is monitored by the muon monitor which measures high energy muons passing through the beam dump. The detector is located in the muon pit, which is located down stream of the beam dump. The proton beam direction can be monitored with an accuracy of better than 1 mrad for each spill by segmented ionization chamber and/or Si pads similar to the system used for K2K. The muon monitor also tracks the stability of the neutrino yield.

4.2 Near detector at 280m from the target

The near detector hall will be located at 280m from the target as shown in Figure 1. The diameter is 20m and the depth is 40m to cover the off-axis angle between 0° to 3σ . The role of the near detectors is to provide predictions of the expected neutrino at the far detector. The near detector is required to have a capability of identifying both event type (CCQE, ν_μ and ν_e inelastic events, neutral current events) and should be able to measure neutrino spectrum at the near location. A fully active fine grained scintillator tracker, similar to the one for the K2K upgrade, is considered as a candidate for the near detector at 280 m. With sufficient granularity, the detector can fully reconstruct quasi-elastic scattering events ($\nu_\mu n \rightarrow \mu^- p$) by tagging recoil protons and identify pions from inelastic scatterings. The detector should have enough radiation length to measure the energies and directions of electrons from the ν_e interaction and π^0 's from the neutral current reactions.

In an ideal case, all the systematic uncertainty would cancel out by using the measured spectra in the near detector. In reality, the near detectors are different from the far detector in terms of material, size (radiation length), and responses. The closer location to the decay pipe also introduces large and complicated far-to-near spectrum ratio. One solution for this challenge is to place a detector far enough away and use very similar detector as the far detector. This will be discussed in the next subsection. Another approach, which can be taken for the 280m detector, is to understand the beam

and the detector responses in detail and correct the differences. Ultimately, systematic uncertainties will be estimated by comparing both of these two approaches

The challenge in understanding the neutrino beam is that only the “product” of neutrino flux, neutrino cross section, and detection efficiency is observable. The flux can be measured by quasi-elastic scattering events, which have clean signature and reliable cross section estimate. Cross sections as a function of the neutrino energy can be measured by placing the near detector at different off-axis locations providing different ν_μ peak energies. Since the scintillator is composed of Carbon, scintillator that contains Oxygen (or water) is considered to measure the cross section difference between Carbon and Oxygen.

Finally, the stability of the beam direction and the flux will be monitored by detecting neutrinos at 0° direction. This measurement complements the measurements by the proton beam monitor and the muon monitor in the beam dump.

5 Intermediate detector

In order to achieve the final designed goals of the experiment, it is important that the front and the far neutrino detectors are designed as similar as possible so that various detector systematics cancel by taking the far-near ratio. The far detector, Super-Kamiokande, is a water Cherenkov detector. Therefore, we propose to construct a front water Cherenkov detector.

By an event rate consideration, we estimate that the fiducial mass of the near detector should be about 100 tons, assuming that the detector is installed at 2 km from the target. We also require that the distance from the surface of the fiducial volume to the photomultiplier tubes (PMTs) is 2.0 m following the definition in Super-Kamiokande. In addition, the near detector has to measure the energy of muons up to about 1 GeV. For this reason, the distance from the surface of the fiducial volume to the PMTs should be about 4 m for the down-stream region. The fiducial volume can be 4 m in diameter and 8 m in length, and the total volume (including the volume for installing PMTs) can be about 9 m in diameter and 15 m in length. The total weight is about 1000 tons.

In addition to the water Cherenkov detector, it is important to install muon range counters at the down stream to measure the energies of high energy muons that shall be produced by the high energy tail of the flux. Furthermore, a fine-grained scintillator detector should be installed in front of the water Cherenkov detector in order to study the details of neutrino interaction kinematics. Figure 4 shows a possible design of the front detector to be installed at about 2 km from the target.

It is known that the energy spectrum of the neutrinos at the Super-Kamiokande detector, which is 295 km away from the neutrino production point, is not necessarily be identical to that at the front detector. For example, Figure 5 compares the calculated energy spectrum at Super-Kamiokande and at 0.28 and 1.5 km distances from the neutrino production target for the 2 degree off-axis beam. 0.28 km is the possible on-site neutrino detector position. The spectrum has lower energy peak at 0.28 km, while the 1.5 km and Super-Kamiokande spectra are almost identical. According to the beam Monte Carlo, the “far-near” ratio ($\equiv \text{flux(far)}/\text{flux(near)} \times (L_{\text{far}}/L_{\text{near}})^2$) approaches to unity very quickly as L_{near} increases, where L_{far} (L_{near}) is the distance between the production target and the far (near) detector. For $L_{\text{near}} > 1.0$ km, the deviation from unity is less than 10%.

From various considerations, 5% far-near systematic error could be the goal for various measurements in the first stage of project. Table 2 shows the expected systematic error in the predicted flux at Super-Kamiokande. It is concluded from this table that the number of events at Super-Kamiokande

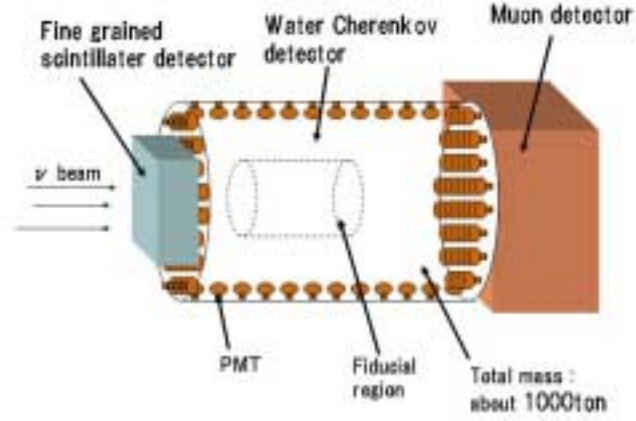


Figure 4: A possible design of the front detector to be installed at about 2 km from the target.

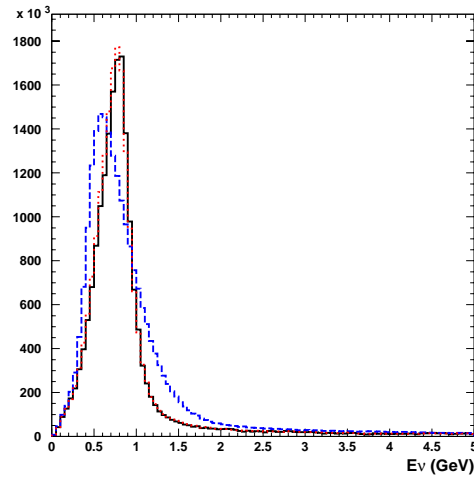


Figure 5: Calculated energy spectrum of the neutrino flux at Super-Kamiokande (solid) and at 0.28 (dashed) and 1.5 km (dotted) distances from the neutrino production target for the 2 degree off-axis beam. The vertical axis is arbitrary.

| Error sources | K2K | JHF with 2km detector |
|---------------|-----------------|-----------------------|
| Spectrum | $\pm 0.6\%$ | |
| non-QE/QE | $+0.5\%/-1.1\%$ | |
| Far-near | $\pm 5\%$ | $< 1\%$ |
| Normalization | $\pm 5\%$ | |
| Total | | |

Table 2: Summary of the expected systematic error in the predicted number of events in Super-Kamiokande. For comparison, the systematic error in K2K is also shown.

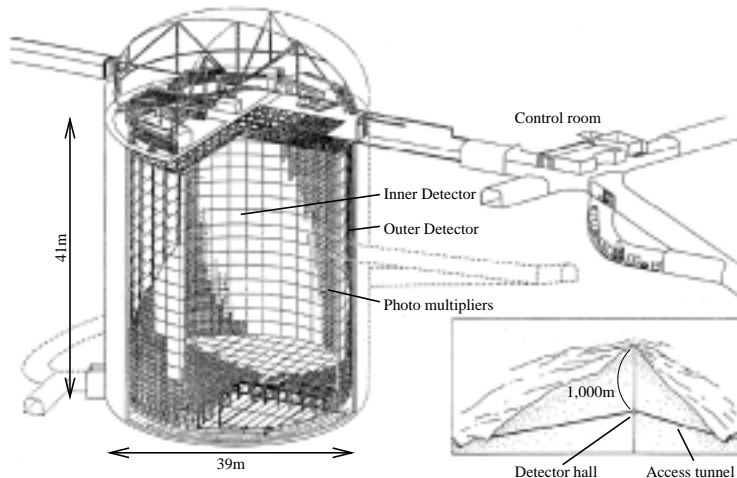


Figure 6: A schematic view of the Super-Kamiokande Detector.

can be predicted within 5 % by the front detector.

6 Far detector: Super-Kamiokande

The Super-Kamiokande Detector is a 50,000 ton water Čerenkov detector located at Kamioka Observatory, Institute for Cosmic Ray Research, the University of Tokyo. The detector will be fully recovered by the start of this experiment. The detector is located beneath the top of Mt. Ikenoyama and the rock over-burden is 1,000 m corresponding to 2,700 meters water equivalent. Super-Kamiokande was commissioned in April 1996 and is running quite stably now.

The detector is optically separated into two parts: the inner detector (ID) and the outer detector (OD). ID is covered with 11,146 20-inch photomultipliers (PMT). The timing and pulse height information of the PMTs are read out by the Analog Timing Modules (ATM).

OD uses 1885 8-inch PMTs and it enables us to distinguish contained neutrino interactions from through-going muons, stopping muons, and neutrino interactions with escaping muons.

Since neutrino interactions located too close to the ID PMTs are difficult to be reconstructed, 22,500 tons of water 2m inside the ID wall is used as the fiducial volume.

A possibly upgrade of the SK detector is foreseen, e.g., to improve a rejection factor of π^0 background, better spatial resolution, efficient tracking of protons, etc.

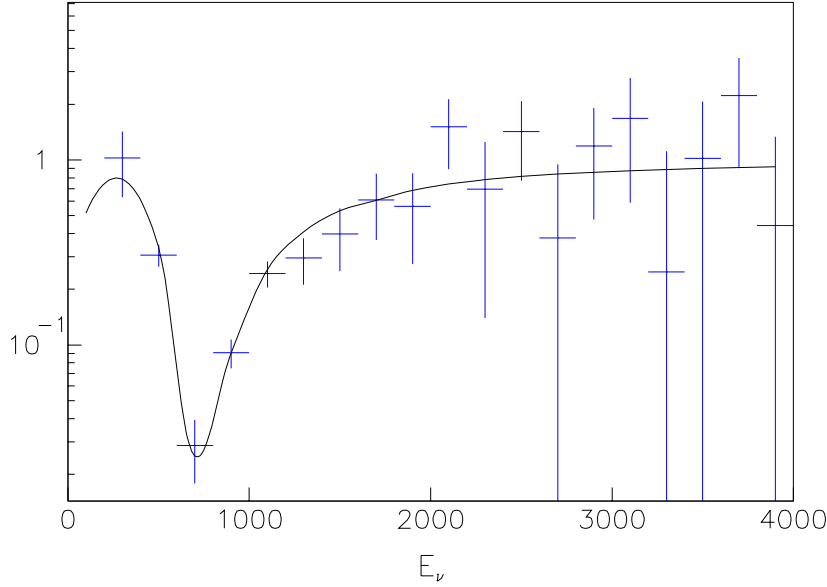


Figure 7: The ratio of the measured spectrum with neutrino oscillation to the expected one without neutrino oscillation after subtracting the contribution of non QE-events. The fit result of the oscillation is overlaid.

7 Physics in the first stage of the project

7.1 High precision measurement of Δm_{23}^2 and θ_{23} with ν_μ disappearance

The neutrino energy can be reconstructed through quasi-elastic (QE) interactions as shown in Equation 1 by the Super-Kamiokande (SK) detector. In this analysis, we use the same muon selection criteria as those used in the atmospheric neutrino analysis by the Super Kamiokande collaboration [5]; fully contained single ring muon-like events in a fiducial volume of 22.5 kt.

In this analysis, the exposure time is five years and θ_{13} is approximated to be zero and thus $1 - \sin^2 2\theta_{\mu\mu} = \sin^2 2\theta_{23}$. The value of θ_{13} will be determined in the $\nu_\mu \rightarrow \nu_e$ search.

In the oscillation analysis, the neutrino energy spectrum is extracted by subtracting the contribution of non-QE background events. To measure the oscillation parameters, full Super-Kamiokande Monte Carlo events are generated. The ratio between the “measured” spectrum at SK and the the expected one without oscillation, after subtracting the non-QE contribution, is fitted by the function of $P(\nu_\mu \rightarrow \nu_\mu)$:

$$P(\nu_\mu \rightarrow \nu_\mu) = 1 - \sin^2 2\theta_{23} \cdot \cos^4 \theta_{13} \cdot \sin^2(1.27\Delta m_{23}^2[eV^2]L[km]/E_\nu[GeV]) \quad (2)$$

Since the spectrum of non-QE events depends on the oscillation parameters, the non-QE spectrum are updated by the fit result at each iteration of the fitting. The survival probability of $P(\nu_\mu \rightarrow \nu_\mu)$ is shown in Figure 7, which gives the fit result of $(\Delta m_{23}^2, \sin^2 2\theta_{23}) = ((2.96 \pm 0.04) \times 10^{-3} \text{eV}^2, 1.0 \pm 0.01)$. The oscillation pattern is clearly seen and the $\sin^2 2\theta_{23}$ precision of 1 % and the Δm_{23}^2 precision of $4 \times 10^{-5} \text{eV}^2$ are expected. Several beam configurations are studied in the range of Δm_{23}^2 between 1×10^{-3} and $1 \times 10^{-2} \text{eV}^2$. The result is summarized in Figure 8. With OA2°, the maximum sensitivity to the oscillation parameters is achieved at $\Delta m_{23}^2 = (3 \sim 3.5) \times 10^{-3} \text{eV}^2$. In the case of $\sin^2 2\theta_{23} = 0.9$, which is the lower bound suggested by atmospheric neutrino result of Super-Kamiokande, the precision is slightly worse due to non-oscillated neutrino events at the oscillation

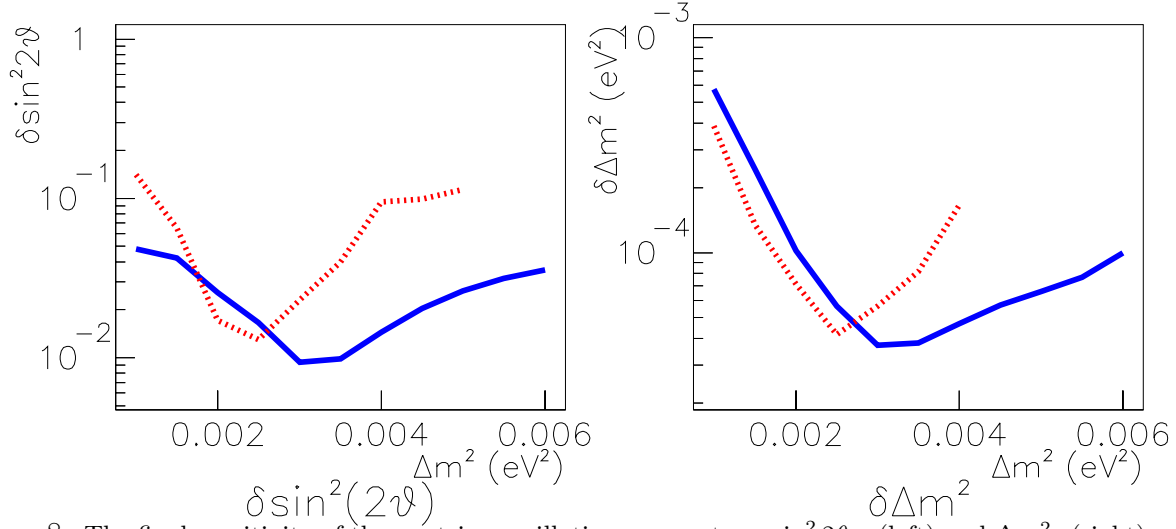


Figure 8: The final sensitivity of the neutrino oscillation parameters: $\sin^2 2\theta_{23}$ (left) and Δm^2_{23} (right), as a function of true Δm^2_{23} (eV²). The $\sin^2 2\theta_{23}$ is set to 1.00. The result with OA2° is shown by the blue (solid) line, OA3° by the red (dashed) line.

maximum. By selecting the bin at the oscillation maximum, the disappearance signal dip is enhanced and thus the contribution of the systematic uncertainties are largely suppressed. For example, the depth of the dip in Figure 7, which corresponds to $1 - \sin^2 2\theta_{23}$, is as small as 3%. Thus, a systematic uncertainty of 10% in the flux normalization (far/near ratio) contributes to $3\% \times 0.1 = 0.3\%$ in the $\sin^2 2\theta_{23}$ measurement. Assuming 10% systematic uncertainty in the far/near ratio, which is similar to K2K's number of 6%, 4% uncertainty in the energy scale, and 20% uncertainty in the non-QE background subtraction, the total systematic error is estimated to be less than 1 % for $\sin^2 2\theta_{23}$ and less than 1×10^{-4} eV² for Δm^2_{23} . The systematic uncertainties are expected to be reduced further below the statistical uncertainties by the neutrino flux measurement using QE events and detailed non-QE background measurement by the front detector, by the pion production measurement, and possibly a second near detector at a few km point which makes the systematics in the far/near ratio negligible.

The overall sensitivity is expected to be 1% in precision for $\sin^2 2\theta_{23}$ and better than 1×10^{-4} eV² for Δm^2_{23} .

7.2 ν_e appearance search

The JHF neutrino beam has small ν_e contamination (0.2% at the peak energy of OAB) and the ν_e appearance signal is enhanced by tuning the neutrino energy at its expected oscillation maximum. Thus, JHFnu experiment has an excellent opportunity to discover ν_e appearance and thus measure θ_{13} . The sensitivity on ν_e appearance is described based on the full Monte Carlo simulations and analysis of Super-Kamiokande and K2K experiments.

The process of the ν_e appearance signal is searched for in the CCQE interaction, for which the energy of neutrino can be calculated to take advantage of the narrow band neutrino beam. Since the proton momentum from the QE interaction is usually below the Čerenkov threshold, the signal has only a single electro-magnetic shower (single ring e-like).

Table 3: Number of events and reduction efficiency of “standard” 1ring e-like cut and π^0 cut for 5 year exposure (5×10^{21} p.o.t.) OA2°. For the calculation of oscillated ν_e , $\Delta m^2 = 3 \times 10^{-3} \text{ eV}^2$ and $\sin^2 2\theta_{\mu e} = 0.05$ is assumed.

| OAB 2° | ν_μ C.C. | ν_μ N.C. | Beam ν_e | Oscillated ν_e |
|--|----------------|----------------|--------------|--------------------|
| 1) Generated in F.V. | 10713.6 | 4080.3 | 292.1 | 301.6 |
| 2) 1R e-like | 14.3 | 247.1 | 68.4 | 203.7 |
| 3) e/π^0 separation | 3.5 | 23.0 | 21.9 | 152.2 |
| 4) $0.4 \text{ GeV} < E_{rec} < 1.2 \text{ GeV}$ | 1.8 | 9.3 | 11.1 | 123.2 |

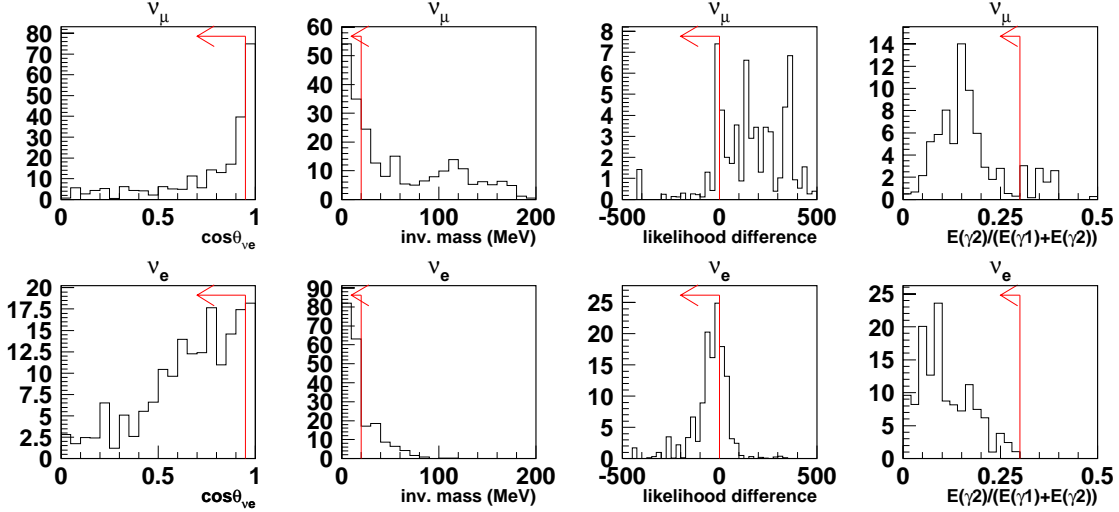


Figure 9: Distributions of the quantities, used in the e/π^0 separation. The beam is the off-axis 2 degree beam and events are after the single-ring e-like selection. Upper histograms corresponds to ν_μ background events and the lower histograms correspond to the ν_e signal events. The arrows in the figure show the cut positions used in the analysis.

The standard Super-Kamiokande atmospheric neutrino analysis are used to select a single ring e-like event: single ring, electron like (showering), visible energy greater than 100 MeV, and no decay electrons. Reduction of number of events by the “standard” 1 ring e-like cut for charged and neutral current events are listed in Table 3. The excellent e/μ separation capability and $\mu \rightarrow e$ detecting capability are key feature of the effective elimination of ν_μ charged current and all of the inelastic events, which contain charged π . The remaining background events at this stage are predominantly from single π^0 production through neutral current interaction and a ν_e contamination. Figure 9 shows distributions of four characteristic quantities that separates signal ν_e events from π^0 background events as follows:

1. Angle between ν and e ($\cos \theta_{\nu e}$):
Some fraction of π^0 background has a steep forward peak, which is likely due to coherent π^0 production. Those events in the extreme forward direction are rejected.
2. Invariant mass of 2 photons:
The π^0 background shows a peak at 135 MeV whereas the ν_e signal shows small invariant mass. Those events with large invariant mass are rejected.
3. Difference between double and single ring likelihood:
For neutrino energies below 1 GeV, the main limitation to separate electrons from π^0 s comes

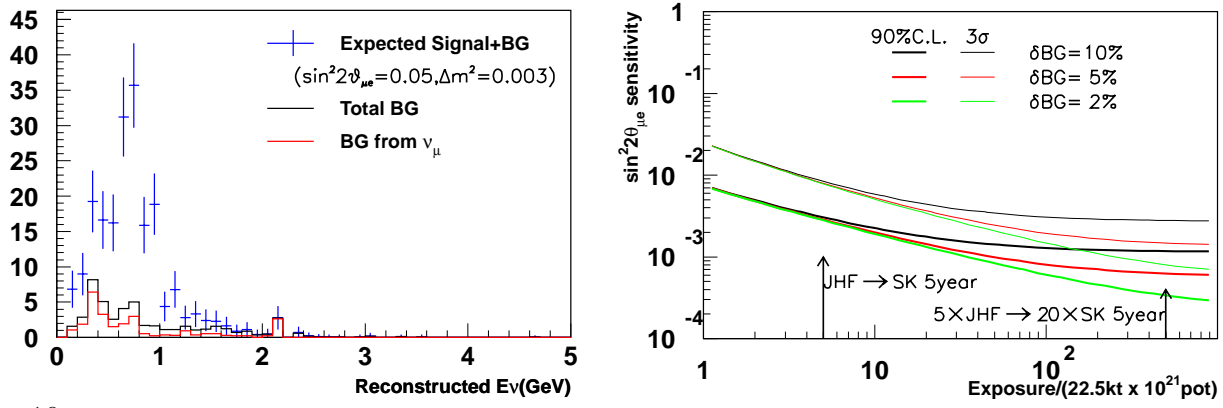


Figure 10: Left: Expected reconstructed neutrino energy distributions of expected signal+BG, total BG, and BG from ν_μ interactions for 5 years exposure of OA2°. Right: Expected (thick lines:) 90%CL sensitivity and (thin lines:) 3σ discovery contours as the functions of exposure time of OA2°. In left figure, expected oscillation signals are calculated with the oscillation parameters: $\Delta m^2 = 3 \times 10^{-3} \text{ eV}^2$, $\sin^2 2\theta_{\mu e} = 0.05$. In right figures, Three different contours correspond to 10%, 5%, and 2% uncertainty in the background estimation.

from asymmetric decay of π^0 s, where the lower energy photon tends to be hidden under the scattered light of the higher energy photon. In order to further suppress the π^0 background, the PMTs hit pattern including scattered light is fitted and two likelihood are calculated; one assuming that the event contains one ring and the other assuming two showing rings. Single ring like events are selected based on the difference of two likelihood.

4. Energy fraction of lower energy ring ($\frac{E(\gamma_2)}{E(\gamma_1)+E(\gamma_2)}$)

The ν_e signal tends to have a low energy second ring which is either a fake ring or a ring due to bremsstrahlung. Those events with the large energy fraction are rejected.

Table 3 lists the number of events after this e/π^0 separation. An order of magnitude extra rejection (247.1/23) in the ν_μ neutral current background is achieved with 152.2/203.7=75% in signal acceptance.

Figure 10 (left) shows the reconstructed neutrino energy distributions for 5 years. The oscillation parameters of $\Delta m^2 = 3 \times 10^{-3} \text{ eV}^2$ and $\sin^2 2\theta_{13} = 0.1$ are assumed. A clear appearance peak is seen at the oscillation maximum of $E_\nu \sim 0.75 \text{ GeV}$. The right plot of Figure 10 show a 90% and 3σ limits as a function of the years of operation with the systematic uncertainty of background subtraction to be 2%, 5% and 10%. The sensitivity of $\sin^2 2\theta_{13} = 0.006$ at 90% confidence level can be achieved in five years of operation. Figure 11 shows 90%CL contours for 5 year exposure of each beam configuration assuming 10% systematic uncertainty in background subtraction.

7.3 Search for sterile neutrinos (ν_s) in ν_μ disappearance

Neutral current (NC) events are the sum of $\nu_\mu \rightarrow \nu_e, \nu_\mu$, and ν_τ oscillations. Therefore, NC measurement combined with $\nu_\mu \rightarrow \nu_e$ and $\nu_\mu \rightarrow \nu_\mu$ measurements provide indirect measurement of the $\nu_\mu \rightarrow \nu_\tau$ and $\nu_\mu \rightarrow \nu_s$ oscillation.

In the JHF sub-GeV neutrino beam, the dominant detectable NC interactions are single π productions. Among those, single π^0 production process is selected to study NC events, because of a unique signature. The following selection criteria are used to select NC π^0 events.

1. The event must be fully contained,

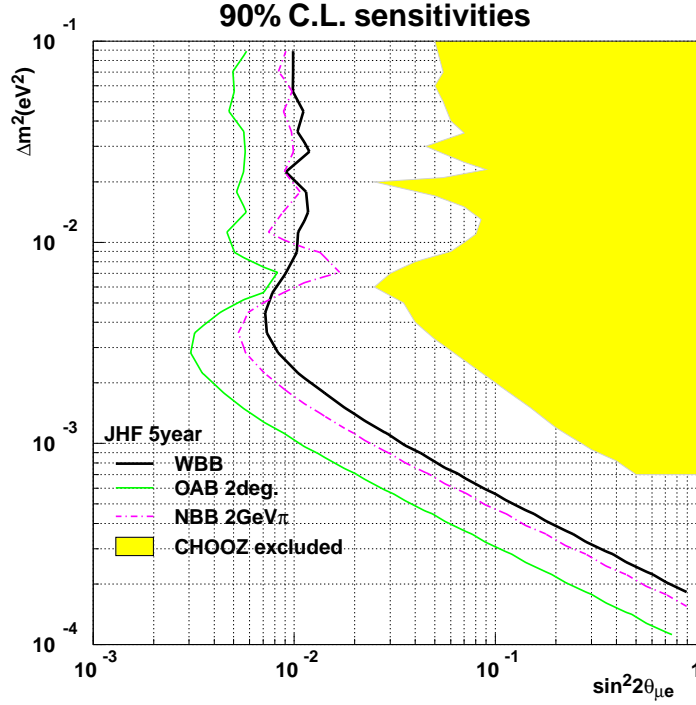


Figure 11: The 90% C.L. sensitivity contours in 5 years of operation with OA2°. The sensitivities with wide band beam and a momentum selected beam are also plotted, The 90% C.L. excluded region of CHOOZ is plotted as a comparison. For CHOOZ contour, maximum mixing of $\sin^2 \theta_{23} = 0.5$ is assumed to convert from $\sin^2 2\theta_{13}$ to $\sin^2 2\theta_{\mu e}$.

Table 4: Summary of the event rate of the NC candidates. $f(X)$ is the fraction of the events from X interaction.

| Beam | #NC Events | Beam exposure | $f(\nu_\mu \text{NC})$ | $f(\nu_\mu \text{CC})$ | $(\nu_e \text{CC})$ |
|------|------------|---------------|------------------------|------------------------|---------------------|
| OA2° | 280 | 5 years | 0.84 | 0.09 | 0.07 |

The total energy deposit in the detector (E_{vis}) is used to reject high energy events. E_{vis} is required to be greater than 100 MeV and less than 1500 MeV.

2. The number of Cherenkov rings in an event must be less than three and they must be electron-like to eliminate background from CC inelastic interactions with a π^0 .
3. No decay electron is required to further eliminate CC events. In the Super-Kamiokande analysis, the efficiency of detecting the decay electrons is better than 85%.

The results are summarized in Table 4.

The expected numbers of events as a function of Δm^2 are shown in Figure 12. In the figures, maximal oscillations, $\sin^2 2\theta_{23}=1.0$, is assumed. The dotted lines in each figure correspond to the 90% C.L. limit for $\nu_\mu \rightarrow \nu_\tau$ oscillations assuming a systematic uncertainty of 5%. The expected numbers of events for $\nu_\mu \rightarrow \nu_\tau$ and for $\nu_\mu \rightarrow \nu_s$ are clearly separated if the Δm^2 is larger than 1×10^{-3} for OAB.

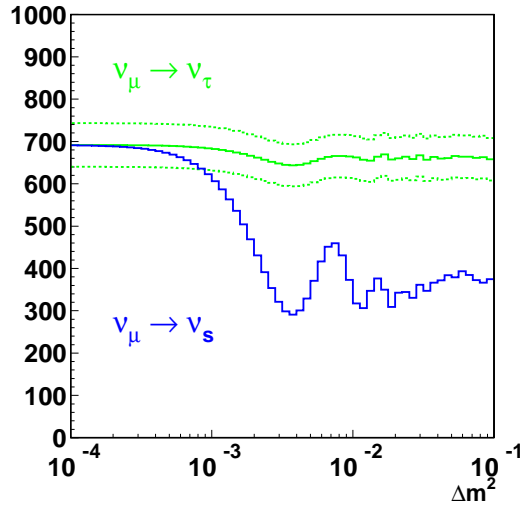


Figure 12: Expected number of events with various Δm^2 for 5 years of OA2°. The solid lines show the expected numbers of events assuming $\nu_\mu \rightarrow \nu_\tau$ or $\nu_\mu \rightarrow \nu_s$. The dotted lines show the 90% C.L. regions of $\nu_\mu \rightarrow \nu_\tau$ oscillation. Although full mixing is assumed, expected number of events does not become 0 even at the deepest dip point. This is due to the NC interactions of high energy neutrinos.

A Neutrino oscillation

The lepton mixing is described by a unitary 3x3 matrix (Maki-Nakagawa-Sakata [3] (MNS) matrix) that is defined by a product of three rotation matrices with three angles (θ_{12} , θ_{23} , and θ_{13}) and complex phase (δ) as in Cabibbo-Kobayashi-Maskawa matrix [4].

$$\begin{pmatrix} \nu_e \\ \nu_\mu \\ \nu_\tau \end{pmatrix} = \begin{bmatrix} U_{\alpha i} \end{bmatrix} \begin{pmatrix} \nu_1 \\ \nu_2 \\ \nu_3 \end{pmatrix}, \quad (3)$$

$$U = \begin{pmatrix} 1 & 0 & 0 \\ 0 & C_{23} & S_{23} \\ 0 & -S_{23} & C_{23} \end{pmatrix} \begin{pmatrix} C_{13} & 0 & S_{13}e^{-i\delta} \\ 0 & 1 & 0 \\ -S_{13}e^{i\delta} & 0 & C_{13} \end{pmatrix} \begin{pmatrix} C_{12} & S_{12} & 0 \\ -S_{12} & C_{12} & 0 \\ 0 & 0 & 1 \end{pmatrix}, \quad (4)$$

where $\alpha = e, \mu, \tau$ are the flavor indices, $i=1, 2, 3$ are the indices of the mass eigenstates, S_{ij} (C_{ij}) stands for $\sin \theta_{ij}$ ($\cos \theta_{ij}$). Neutrinos are produced as flavor eigenstates and each component of mass eigenstates gets a different phase after traveling a certain distance. The detection of neutrino by charged current interactions projects these new state back onto flavor eigenstates. The probability of oscillation is given by the formula,

$$P(\nu_\alpha \rightarrow \nu_\beta) = \delta_{\alpha\beta} - 4 \sum_{i>j} \text{Re}(U_{\alpha i}^* U_{\beta i} U_{\alpha j} U_{\beta j}^*) \cdot \sin^2 \Phi_{ij} \pm 2 \sum_{i>j} \text{Im}(U_{\alpha i}^* U_{\beta i} U_{\alpha j} U_{\beta j}^*) \cdot \sin 2\Phi_{ij} \quad (5)$$

where

$$\Phi_{ij} \equiv \Delta m_{ij}^2 L / 4E_\nu = 1.27 \Delta m_{ij}^2 [eV^2] L [km] / E_\nu [GeV], \quad (6)$$

$\Delta m_{ij}^2 = m_j^2 - m_i^2$, L is the flight distance, and E_ν is the neutrino energy. The \pm sign in the third term is the CP violation effect, $-$ for neutrinos and $+$ for anti-neutrinos. Because $\Delta m_{12}^2 + \Delta m_{23}^2 + \Delta m_{31}^2 = 0$,

there exist only two independent Δm^2 for three species of neutrinos. Thus 3 generation neutrino oscillation can be described by two Δm^2 's, three angles ($\theta_{12}, \theta_{23}, \theta_{13}$) and one phase (δ).

We take the two Δm^2 values as the values suggested by solar and atmospheric neutrino measurements; $\Delta m_{12}^2 \equiv \Delta m_{sol}^2 \simeq 10^{-4} \rightarrow 10^{-10} \text{ eV}^2$ and $\Delta m_{23}^2 \simeq \Delta m_{31}^2 \equiv \Delta m_{atm}^2 = (1.6 \sim 4) \times 10^{-3} \text{ eV}^2$. For an oscillation measurement with $E_\nu \simeq \Delta m_{23}^2 \cdot L$ as in this proposed experiment, the contribution of Δm_{12}^2 term is small and the oscillation probabilities can be approximately expressed by two mixing angles;

$$P(\nu_\mu \rightarrow \nu_e) = \sin^2 2\theta_{13} \cdot \sin^2 \theta_{23} \cdot \sin^2 \Phi_{23}, \quad (7)$$

$$P(\nu_\mu \rightarrow \nu_\mu) = 1 - \sin^2 2\theta_{23} \cdot \cos^4 \theta_{13} \cdot \sin^2 \Phi_{23} - P(\nu_\mu \rightarrow \nu_e), \quad (8)$$

$$P(\nu_e \rightarrow \nu_\tau) = \sin^2 2\theta_{13} \cdot \cos^2 \theta_{23} \cdot \sin^2 \Phi_{23}, \quad (9)$$

$$P(\nu_e \rightarrow \nu_e) = 1 - \sin^2 2\theta_{13} \cdot \sin^2 \Phi_{23}. \quad (10)$$

If we define effective mixing angles as $\sin^2 2\theta_{\mu e} \equiv \sin^2 2\theta_{13} \cdot \sin^2 \theta_{23}$ and $\sin^2 2\theta_{\mu\tau} \equiv \sin^2 2\theta_{23} \cdot \cos^4 \theta_{13}$, then the expressions reduce to the ones in the two flavor approximation;

$$3P(\nu_\mu \rightarrow \nu_e) = \sin^2 2\theta_{\mu e} \cdot \sin^2 \Phi_{23}, \quad (11)$$

$$P(\nu_\mu \rightarrow \nu_\mu) = 1 - \sin^2 2\theta_{\mu\tau} \cdot \sin^2 \Phi_{23} - P(\nu_\mu \rightarrow \nu_e). \quad (12)$$

Experimental constraints obtained from ν_μ disappearance in the atmospheric neutrino are $\sin^2 2\theta_{\mu\tau} > 0.89$ and $1.6 \times 10^{-3} < \Delta m_{23}^2 < 4 \times 10^{-3} \text{ eV}^2$ [5]. Solar neutrino observations allow The Large mixing angle solution: LMA, $2.5 \times 10^{-5} \text{ eV}^2 < \Delta m^2 < 3.3 \times 10^{-4} \text{ eV}^2$, $0.25 < \tan^2 \theta < 0.9$ at 3σ bounds. The most stringent constraint on θ_{13} comes from reactor $\bar{\nu}_e$ disappearance experiments. As can be seen in eq. (10), $\bar{\nu}_e$ disappearance directly measures θ_{13} . The current limit is $\sin^2 2\theta_{13} < 0.05$ for $\Delta m_{23}^2 \simeq 6 \times 10^{-3} \text{ eV}^2$ and $\sin^2 2\theta_{13} \leq 0.12$ for $\Delta m_{23}^2 \simeq 3 \times 10^{-3} \text{ eV}^2$ at 90 % C.L [16]. Since θ_{13} is very small and atmospheric neutrino data indicates almost full mixing $\theta_{23} \simeq \pi/4$, the effective two flavor mixing angles defined above and 3 flavor angles have following approximate relations;

$$\sin^2 2\theta_{\mu\tau} \simeq \sin^2 2\theta_{23}, \quad \sin^2 2\theta_{\mu e} \simeq \frac{1}{2} \sin^2 2\theta_{13} \simeq 2 |U_{e3}|^2. \quad (13)$$

It follows from eq. (5) that CP violation can be observed only with appearance experiments, since $\text{Im}(U_{\alpha i}^* U_{\beta i} U_{\alpha j} U_{\beta j}^*) = 0$ for $\alpha = \beta$. Especially $\nu_\mu \leftrightarrow \nu_e$ oscillation is known to provide the best chance in measuring the CP asymmetry in lepton sector. This is because the leading CP conserving term of $\nu_\mu \leftrightarrow \nu_e$ oscillation is highly suppressed due to small Δm_{12}^2 and the subleading terms, such as U_{e3} related and CP violating terms, give leading contributions, as shown below. If the oscillation $\nu_\mu \rightarrow \nu_e$ is at the observable level in the first phase of the project, further investigation of CP violation will be carried out in the second phase. In addition since CP violation in three generations requires that all three members should be involved in the process, solar neutrino related quantities (θ_{12}, Δ_{12}) must be large (namely large mixing angle solution for solar neutrino oscillation) in order for the CP violation of the neutrino oscillation to be observable.

The $\nu_\mu \rightarrow \nu_e$ appearance probability can be written using MNS matrix element as [17]

$$\begin{aligned} 1P(\nu_\mu \rightarrow \nu_e) = & 4C_{13}^2 S_{13}^2 S_{23}^2 \sin^2 \Phi_{31} \\ & + 8C_{13}^2 S_{12} S_{13} S_{23} (C_{12} C_{23} \cos \delta - S_{12} S_{13} S_{23}) \cos \Phi_{32} \cdot \sin \Phi_{31} \cdot \sin \Phi_{21} \\ & - 8C_{13}^2 C_{12} C_{23} S_{12} S_{13} S_{23} \sin \delta \sin \Phi_{32} \cdot \sin \Phi_{31} \cdot \sin \Phi_{21} \\ & + 4S_{12}^2 C_{13}^2 (C_{12}^2 C_{23}^2 + S_{12}^2 S_{23}^2 S_{13}^2 - 2C_{12} C_{23} S_{12} S_{23} S_{13} \cos \delta) \sin^2 \Phi_{21} \\ & - 8C_{13}^2 S_{13}^2 S_{23}^2 (1 - 2S_{13}^2) \frac{aL}{4E_\nu} \cos \Phi_{32} \sin \Phi_{31}. \end{aligned} \quad (14)$$

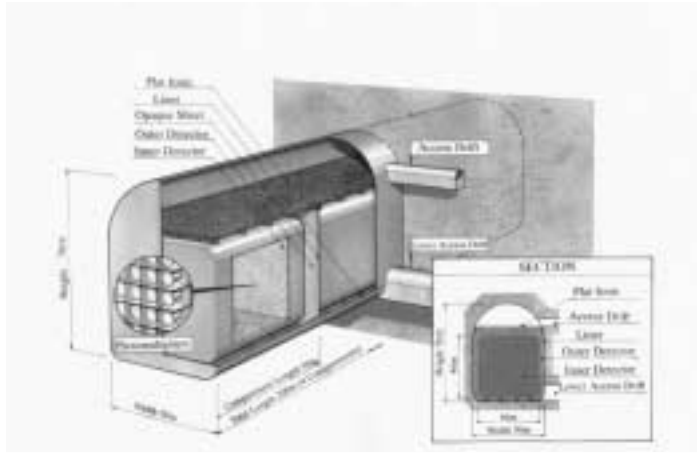


Figure 13: Schematic view of the Hyper-Kamiokande detector.

The first term has the largest contribution. The second $\cos\delta$ term is generated by CP phase δ but CP conserving. The third $\sin\delta$ term violates CP. The fourth term, which is the solar neutrino term, is suppressed by $\sin^2 \frac{\Delta m_{21}^2 L}{4E_\nu}$. The matter effect is characterized by

$$a = 2\sqrt{2}G_F n_e E_\nu = 7.6 \times 10^{-5} \rho [g/cm^3] E_\nu [GeV] \quad [eV^2], \quad (15)$$

where G_F is the Fermi constant, n_e is the electron density and ρ is the earth density. The probability $P(\bar{\nu}_\mu \rightarrow \bar{\nu}_e)$ is obtained by the replacing $a \rightarrow -a$ and $\delta \rightarrow -\delta$ in eq. (14). As seen in eq. (15) the matter effect is proportional to neutrino energy, so the lower the energy, the smaller the effect is. The CP asymmetry in the absence of matter effect is calculated as

$$A_{CP} = \frac{P(\nu_\mu \rightarrow \nu_e) - P(\bar{\nu}_\mu \rightarrow \bar{\nu}_e)}{P(\nu_\mu \rightarrow \nu_e) + P(\bar{\nu}_\mu \rightarrow \bar{\nu}_e)} \simeq \frac{\Delta m_{12}^2 L}{4E_\nu} \cdot \frac{\sin 2\theta_{12}}{\sin \theta_{13}} \cdot \sin \delta \quad (16)$$

Because θ_{13} is small, CP asymmetry can be large, especially for small E_ν .

B Physics in the future extension with Hyper-Kamiokande

In the 2nd phase of the JHF-Kamioka neutrino experiment, the proton intensity is planned to go up to 4 MW [18]. The pion (or neutrino) production target will also be upgraded to a liquid metal target to accept the 4 MW beam. The shielding of the decay pipe will be designed to accommodate such a beam.

As for the far detector, Hyper-Kamiokande detector is proposed as a next generation large water Čerenkov detector [19] at Tochibora zinc mine in Kamioka, which is about 8 km south of the Super-Kamiokande detector. Schematic view of one candidate detector design is shown in Figure 13. A 500 m long water tank is made from 10 sub-detectors with 50 m long each. The tank will be filled with pure water and photomultiplier tubes (PMTs) are instrumented on all surfaces of sub-detectors. The fiducial volume of the detector is about 0.54 Mt. The outer detectors with the thickness of at least 2.0 m completely surround the inner sub-detectors and the outer region is also instrumented with PMTs. The primary function of the outer detectors is to veto cosmic ray muons and to help identify contained events. The Kamioka site satisfies the conditions required for constructing large water Čerenkov detectors: easy access to underground, clean water, hard and uniform rock, and

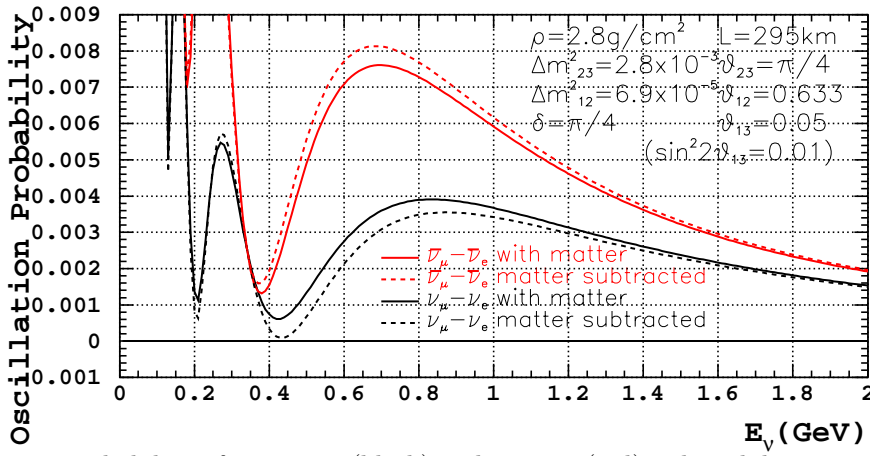


Figure 14: Oscillation probabilities for $\nu_\mu \rightarrow \nu_e$ (black) and $\bar{\nu}_\mu \rightarrow \bar{\nu}_e$ (red). The solid curves includes asymmetry due to matter effect. For the dashed curves, the matter effect is subtracted and the difference between $\nu_\mu \rightarrow \nu_e$ (black) and $\bar{\nu}_\mu \rightarrow \bar{\nu}_e$ (red) are all due to CP effect.

infrastructure/technology for excavation. The overburden of the Hyper-Kamiokande is expected to be about 1500 meter-water-equivalent.

With these upgrades in both accelerator ($\times 5$) and detector ($\times 25$), the statistics is expected to increase by more than a factor of 100. The goal of the second phase is

- $\sin^2 2\theta_{13}$ sensitivity below 10^{-3}
- CP phase δ measurement down to 10-20 degrees
- Test of the unitarity triangle in the lepton sector
- Search for Proton decay: $p \rightarrow K^+ \bar{\nu}, e^+ \pi^0$

B.1 Discovery potential of CP violation in the lepton sector

If $\nu_\mu \rightarrow \nu_e$ is not observed in the first phase, another order of magnitude improvement in $\sin^2 2\theta_{\mu e}$ sensitivity to better than 10^{-3} will be performed in the second phase (Fig 10). Systematic uncertainty in background subtraction becomes important in the 2nd phase. Enhancement of the signal at the oscillation maximum and capability of measuring the background by the side-band of the oscillation pattern in the reconstructed neutrino energy distribution provide an excellent handle in controlling the systematic uncertainty.

Now that the large mixing angle solution of the solar neutrino deficit is confirmed by KamLAND, the chance of discovering CP violation is good providing that θ_{13} and δ_{CP} are not suppressed too much. The CP asymmetry is calculated as

$$A_{CP} = \frac{P(\nu_\mu \rightarrow \nu_e) - P(\bar{\nu}_\mu \rightarrow \bar{\nu}_e)}{P(\nu_\mu \rightarrow \nu_e) + P(\bar{\nu}_\mu \rightarrow \bar{\nu}_e)} = \frac{\Delta m_{12}^2 L}{4E_\nu} \cdot \frac{\sin 2\theta_{12}}{\sin \theta_{13}} \cdot \sin \delta$$

By choosing low energy neutrino beam at the oscillation maximum ($E \sim 0.75$ GeV and $L \sim 295$ km for JHF) the CP asymmetry is enhanced as $1/E$. Taking the best fit values of KamLAND, $\sin^2 2\theta_{12} = 0.91$ and $\Delta m_{12}^2 = 6.9 \times 10^{-5}$, $1/10$ of the CHOOZ limit for $\sin^2 2\theta_{13} = 0.01$, and $\delta = \pi/4$ (half of the maximum CP angle), A_{CP} becomes as large as 40% as shown in Figure 14. Matter effect, which creates fake CP asymmetry, increases linearly with the neutrino energy. Because of the use of low energy neutrinos, the fake asymmetry due to matter effect is small for the JHF-Kamioka experiment.

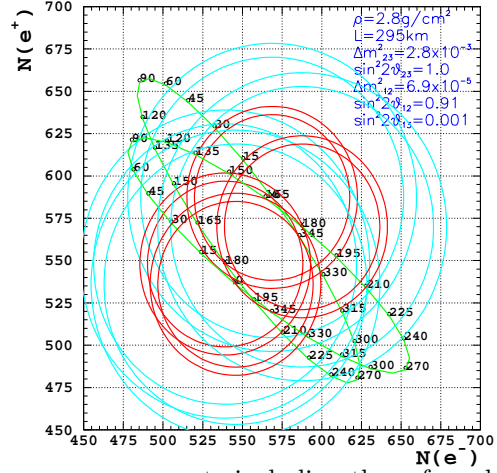
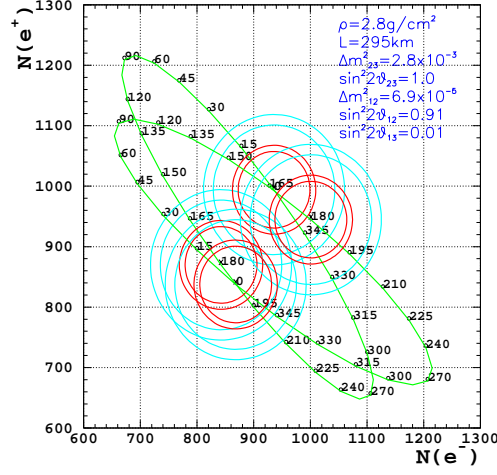
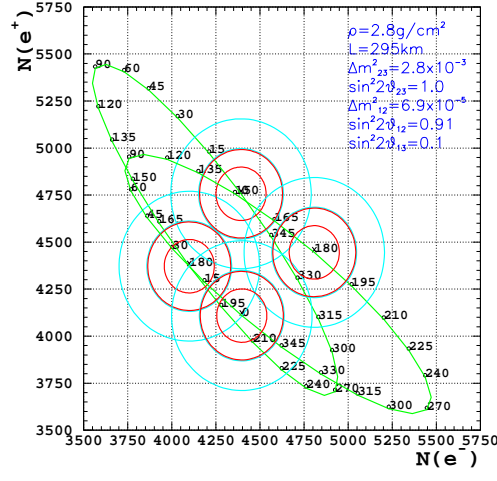


Figure 15: Numbers of ν_e and $\bar{\nu}_e$ appearance events including those from backgrounds for $\sin^2 2\theta_{13}=0.1, 0.01$, and 0.001 . Each of the two green contours corresponds to the different mass hierarchy and the numbers on the contour are the CP phase in degree. The red circles corresponds to the 90% contours and the blue circles are the 3σ contours after 2 years of ν_μ and 6 years of $\bar{\nu}_\mu$ runs. The outer circles includes errors due to 2% systematic uncertainty.

Figure 15 shows the numbers of ν_e and $\bar{\nu}_e$ appearance events including those from backgrounds after 6 years of $\bar{\nu}_\mu$ and 2 years of ν_μ running in the 2nd phase of the JHF-Kamioka neutrino experiment.

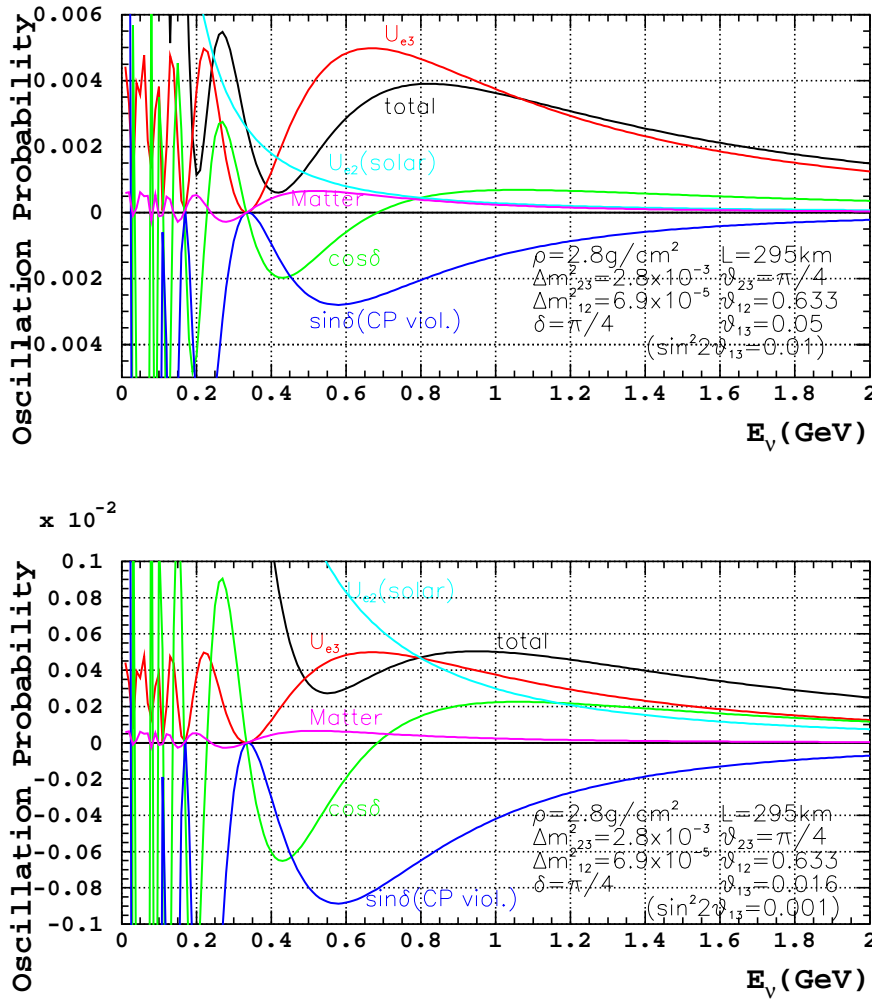


Figure 16: Contribution of different component to $\nu_\mu \rightarrow \nu_e$ appearance $\sin^2 2\theta_{13}=0.01$ and 0.001 .

The top plot corresponds to the CHOOZ limit of $\sin^2 2\theta_{13}=0.1$ and the middle and the bottom plots correspond to $\sin^2 2\theta_{13}=0.01$ and 0.001 , respectively. Numbers on the plots indicates CP phase δ in degrees. CP phase at 0 degrees and 180 degrees correspond to no CP violation. 3 sigma discovery is possible for $|\delta| > 20^\circ$ for $\sin^2 2\theta_{13} > 0.01$. There is a significant CP sensitivity left even at $\sin^2 2\theta_{13}=0.001$.

Figure 16 shows the contributions of each of the terms in $\nu_\mu \rightarrow \nu_e$ appearance for $\sin^2 2\theta_{13}=0.01$ and 0.001 . Interestingly, CP violating contribution provides the largest contribution in the case of $\sin^2 2\theta_{13}=0.001$. Because contribution of these terms are all significant, each of the components in Eq (14) could be determined by measuring the oscillation pattern of the $\nu_\mu \rightarrow \nu_e$ and $\bar{\nu}_\mu \rightarrow \bar{\nu}_e$ appearances. This oscillation pattern provides 4 independent measurements of the MNS matrix elements and can over-constrain the unitary triangle: $U_{e1}^* U_{\mu 1} + U_{e2}^* U_{\mu 2} + U_{e3}^* U_{\mu 3} = 0$ [20].

B.2 Sensitivity of proton decay

The existence of the neutrino oscillation indicates the extremely small neutrino masses, which is 12-13 orders of magnitude smaller than the top quark mass. A natural way to explain this hierarchy is Grand Unified theories (with see-saw mechanism), which is also indicated by the running gauge coupling constants. The only known way to directly observe the grand unification phenomenon is a nucleon decay measurement. The main gauge-boson-mediated decay is $p \rightarrow e^+ \pi^0$ and the predicted

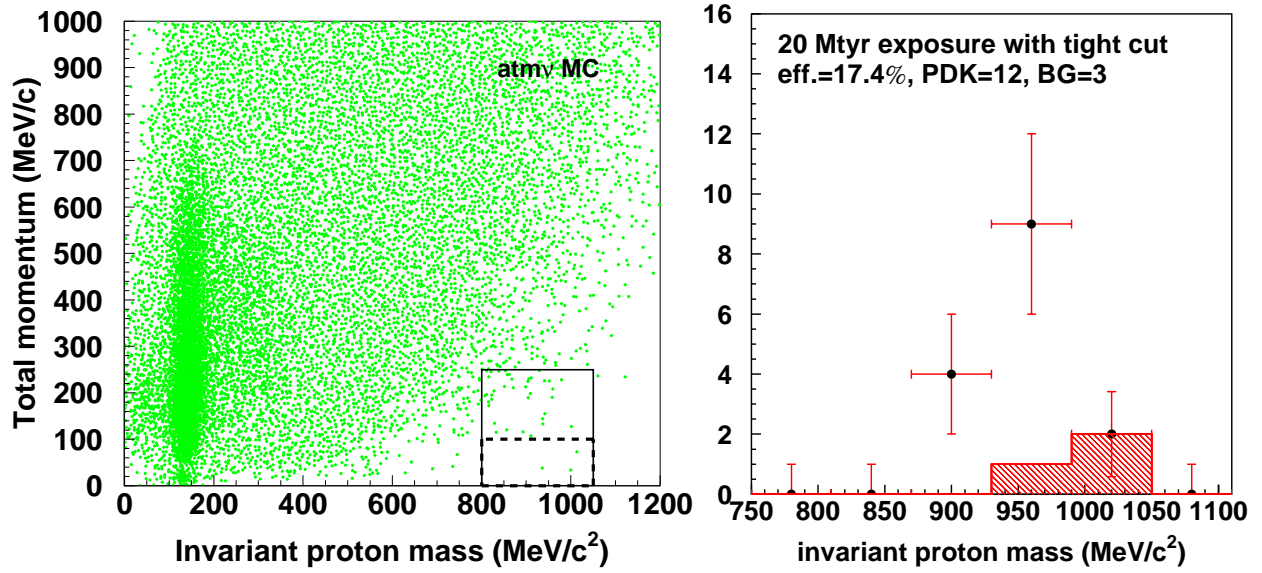


Figure 17: Left: Observed invariant proton mass and total momentum distributions for simulated atmospheric neutrino backgrounds of 20 Mt-year exposure. Solid box shows traditional selection criterion used in Super-Kamiokande [24]. Dashed box shows new tighter cut for reducing background. Right: Observed invariant proton mass distributions for 20 Mt-year exposure. Partial proton lifetime for $p \rightarrow e^+\pi^0$ is assumed to be 1×10^{35} years.

lifetime could be as short as $\sim 10^{35}$ years [21]. For supersymmetric grand unified theories, $p \rightarrow \bar{\nu}K^+$ decay tends to be the main decay mode and its predicted life time is somewhere between $10^{32} - 10^{35}$ years, although this decay mode is highly model dependent. For both of these modes, it is highly desirable to reach the sensitivity of $\sim 10^{35}$ years and beyond. Current lower limits on partial lifetimes of these two modes from 92 kton-year of Super-Kamiokande data [22] are

$$\tau_p/B_{p \rightarrow e^+\pi^0} > 5.7 \times 10^{33} \text{ years (90\% confidence level)}$$

$$\tau_p/B_{p \rightarrow \bar{\nu}K^+} > 2.0 \times 10^{33} \text{ years (90\% confidence level)}$$

where τ_p is the proton lifetime and B is the branching ratio of the decay mode.

In the following sensitivity study [23], the neutrino interaction simulation and detector simulation used in Super-Kamiokande are used. Figure 17 shows simulated atmospheric neutrino backgrounds for 20 Mt-year exposure. The solid box shows the signal region used in Super-Kamiokande [24]. An estimated number of background events is 45 for 20 Mt-year and it appears that background limits the statistics in the future $p \rightarrow e^+\pi^0$ search and a tighter cut is desired.

In the water molecule, 2 out of 10 protons are free protons. These free protons have no Fermi motion and thus give sharp proton mass peak in $e^+\pi^0$ invariant mass distribution (x-axis) and nearly perfect momentum balance (y-axis). The detection efficiency is also higher because of no pion interaction loss in the Oxygen nucleus. The dashed box in the figure represents a tighter selection criterion in momentum balance to select only the free proton decay. The background level is reduced by a factor of 15, or 3 background events/20 Mt-year, whereas the 39% of the signal detection efficiency is maintained. The overall signal detection efficiency is 17.4%. Figure 17(right) shows the expected invariant mass distribution for 20 Mt-year exposure data, assuming a partial lifetime for the proton of 1×10^{35} years and the tight cut described above. A sharp peak at the proton mass is seen, which would provide a redundant positive evidence of proton decay. Figure 18(left) shows 99.73%(3 σ) discovery sensitivity. With 20 Mt-year exposure, we will reach a sensitivity beyond 10^{35} years.

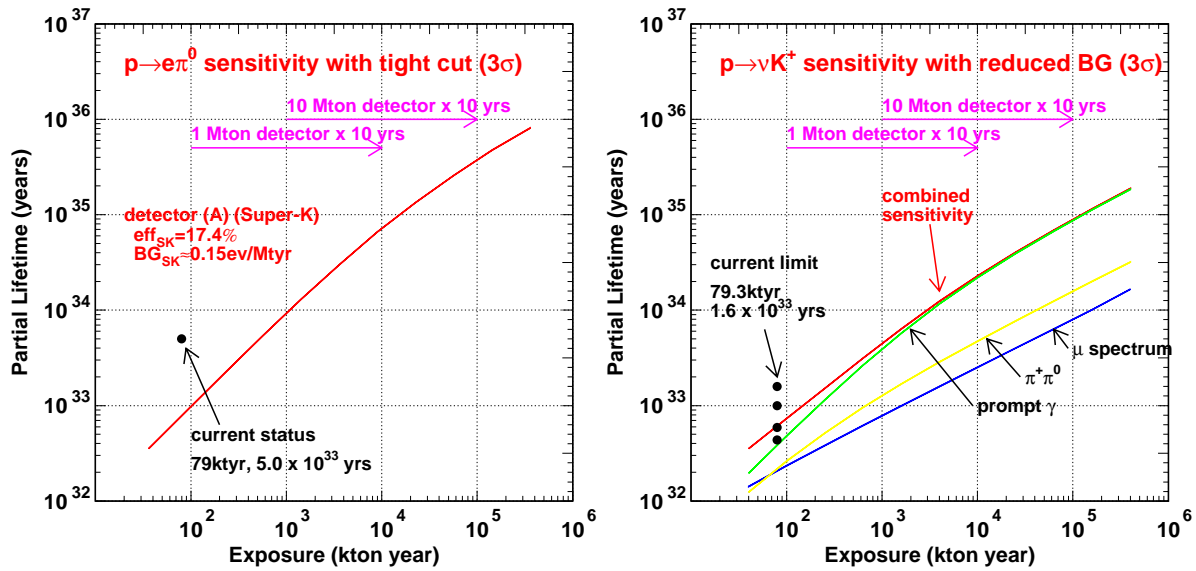


Figure 18: Expected sensitivity for the partial lifetime of protons as a function of detector exposure. In the left figure, the sensitivity for $p \rightarrow e^+\pi^0$ is calculated at 99.73%(3σ) confidence level. The tight momentum cut (see text) is used in the calculation. The right figure shows the expected sensitivity for $p \rightarrow \bar{\nu}K^+$ mode. Background is assumed to be reduced for muon and prompt gamma tagging method (see text). The upper line shows the combined sensitivity for this decay mode.

For the $p \rightarrow \bar{\nu}K^+$ search, Super-Kamiokande developed a nearly background free method of detecting μ^+ from a $K \rightarrow \mu\nu$ decay accompanied by a prompt γ from the residual oxygen nucleus [25]. The backgrounds for this prompt γ tagging is assumed to come from kaon production by atmospheric neutrinos. Figure 18(right) shows 99.73%(3σ) discovery sensitivity for the $p \rightarrow \bar{\nu}K^+$ search. With 20 Mt-year exposure, we will reach a sensitivity of 3×10^{34} years, closing (or opening?) the windows for many of the supersymmetric grand unified theories.

References

- [1] R.H. Frampton, S.L. Glashow, T. Yanagida hep-ph/0208157
- [2] Y. Itow et.al. The JHF-Kamioka neutrino Project hep-ex/0106019
- [3] Z. Maki, M. Nakagawa, S.Sakata, Prog. Theor. Phys. 28,870 (1962)
- [4] M.Kobayashi, T. Maskawa, Prog. Theor. Phys. 49,652 (1973)
- [5] Super-Kamiokande collaboration, Phys.Rev.Lett. 81,1562 (1998)
- [6] K2K collaboration, hep-ex/0212007, accepted for publication in Phys.Rev.Lett.
- [7] Super-Kamiokande collaboration, Phys.Rev.Lett.85,3999 (2000)
- [8] SNO Collaboration, Phys.Rev.Lett.89,011301(2002)
- [9] The Super-Kamiokande collaboration, hep-ex/0103032, hep-ex/0103033, to appear in Phys. Rev. Lett.
- [10] KamLAND Collaboration. hep-ex/0212021

- [11] For example, Yamanoi Y. et al., KEK Preprint 97-225, November 1997.
- [12] D. Beavis, A. Carroll, I. Chiang, *et al.*, Proposal of BNL AGS E-889 (1995).
- [13] R. Brun et al., CERN DD/EE/84-1 (1987).
- [14] T.A.Gabriel et al., ORNL/TM-11185; C.Zeitnitz and T.A.Gabriel, Nucl. Instr. and Meth. **A349**, 106 (1994).
- [15] K. Nishikawa, talk presented at KEK-PS review, Dec., 2000; T. Nakaya, talk presented at 2001 Lake Louise Winter Institute, Feb., 2001.
- [16] CHOOZ: Apollonio M. et al., Phys. Lett. **B466** (B1999) 415. Palo Verde:F. Boehm *et al.*, Nucl.Phys.Proc.Suppl. 91:91(2001)
- [17] B. Richter, SLAC-PUB-8587 (hep-ph/0008222), 2000 and references there in.
- [18] M. Furusaka, R. Hino, Y. Ikeda *et al.*, “*The Joint Project for High-Intensity Proton Accelerators*”, KEK Report 99-4; JAERI-Tech 99-056; JHF-99-3 (1999).
- [19] M. Koshiha, *Phys. Rep.* **220**, 229 (1992); K. Nakamura, talk presented at Int. Workshop on Next Generation Nucleon Decay and Neutrino Detector, 1999, SUNY at Stony Brook; K. Nakamura, *Neutrino Oscillations and Their Origin*, (Universal Academy Press, Tokyo, 2000), p. 359.
- [20] J. Sato, hep-ph/0008056 (2000).
- [21] W. Marciano, talk presented at UNO proto-collaboration meeting, 2000, Carlsbad, USA.
- [22] M. Shiozawa, talk presented at the 30th Int. Conf. on High Energy Physics (ICHEP2000), 2000, Osaka, Japan.
- [23] M. Shiozawa, *Next Generation Nucleon Decay and Neutrino Detector(NNN99)* (AIP Conference Proceedings 533, AIP, New York, 2000) p.21; M. Shiozawa, talk presented at Int. Workshop on Next Generation Nucleon Decay and Neutrino Detector, 2000, Fermi National Laboratory, USA.
- [24] M. Shiozawa *et al.*, *Phys. Rev. Lett.* **81**, 3319 (1998).
- [25] Y. Totsuka, *7th Workshop on Grand Unification, ICOBAN '86*, (World Scientific, 1986), p. 118; Y. Hayato *et al.*, *Phys. Rev. Lett.* **83**, 1529 (1999).